

1 Version 0.1 DRAFT

# 2 ATLAS+CMS DARK MATTER FORUM RECOMMENDA- 3 TIONS

4 Author/contributor list to be added as document is finalized.

5 May 4, 2015



<sup>6</sup> ***1***

<sup>7</sup> *Introduction*

<sup>8</sup> This is a citation test [HK11].



9 2

10 *Overall choices for simplified models*

11 General topics:

- 12 • choice of Dark Matter type: Dirac (unless specified otherwise) and  
13 what we might be missing
- 14 • MFV and what we might be missing



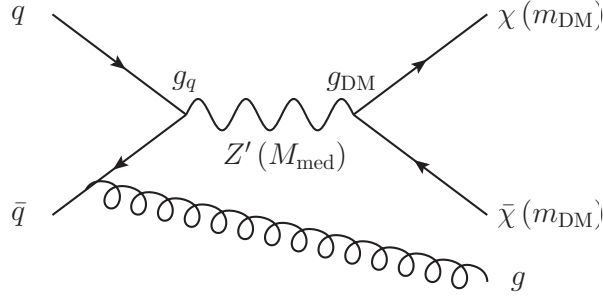


Figure 3.1: The diagram shows the pair production of dark matter particles in association with a parton from the initial state via an s-channel vector or axial-vector mediator. The process is specified by  $(M_{\text{med}}, m_{\text{DM}}, g_{\text{DM}}, g_q)$ , the mediator and dark matter masses, and the mediator couplings to dark matter and quarks respectively.

3

## Recommended models for all MET+X analyses

### 3.1 Vector and axial vector mediator, s-channel exchange

There are several matrix element implementations of the s-channel vector mediated DM production. This is available in POWHEG, MADGRAPH and also MCFM. The implementation in POWHEG generates DM pair production with 1 parton at next-to-leading order (NLO), whilst MADGRAPH and MCFM are at leading order (LO). As shown in POWHEG Ref. [HKR13], including NLO corrections result in an enhancement in the cross section as compared to LO and though this is not significant, it does lead to a substantial reduction in the dependence on the choice of the renormalization and factorization scale and hence the theoretical uncertainty on the signal prediction. Since NLO calculations are available for the process in POWHEG, we recommend to proceed with POWHEG as the generator of choice.

We consider the case of a dark matter particle that is a Dirac fermion and where the production proceeds via the exchange of a spin-1 s-channel mediator. We consider the following interactions between the DM and SM fields including a vector mediator with:

- (a) vector couplings to DM and SM,
- (b) axial-vector couplings to DM and SM.

The corresponding Lagrangians are

$$\mathcal{L}_{\text{vector}} = \sum_q g_q Z'_\mu \bar{q} \gamma^\mu q + g_{\text{DM}} Z'_\mu \bar{\chi} \gamma^\mu \chi \quad (3.1)$$

$$\mathcal{L}_{\text{axial-vector}} = \sum_q g_q Z'_\mu \bar{q} \gamma^\mu \gamma^5 q + g_{\text{DM}} Z'_\mu \bar{\chi} \gamma^\mu \gamma^5 \chi \quad (3.2)$$

where the coupling extends over all the quarks and universal couplings are assumed for all the quarks. It is also possible to consider another model in which mixed vector and axial-vector couplings are considered, for instance the couplings to the quarks are vector whereas those to DM are axial-vector. As a starting point, we consider only the models with the vector couplings only and axial vector couplings only.

We assume that no additional visible or invisible decays contribute to the width of the mediator, this is referred to as the minimal width and it is defined as follows for the vector and axial-vector models.

$$\Gamma_{\text{min}} = \Gamma_{\bar{\chi}\chi} + \sum_q \Gamma_{\bar{q}q} \quad (3.3)$$

where the individual contributions to this from the partial width are from

$$\Gamma_{\bar{\chi}\chi}^V = \frac{g_{\text{DM}}^2 M_{\text{med}}}{12\pi} \left( 1 + \frac{2m_{\text{DM}}^2}{M_{\text{med}}^2} \right) \sqrt{1 - \frac{4m_{\text{DM}}^2}{M_{\text{med}}^2}} \quad (3.4)$$

$$\Gamma_{\bar{q}q}^V = \frac{3g_q^2 M_{\text{med}}}{12\pi} \left( 1 + \frac{2m_q^2}{M_{\text{med}}^2} \right) \sqrt{1 - \frac{4m_q^2}{M_{\text{med}}^2}} \quad (3.5)$$

$$\Gamma_{\bar{\chi}\chi}^A = \frac{g_{\text{DM}}^2 M_{\text{med}}}{12\pi} \left( 1 - \frac{4m_{\text{DM}}^2}{M_{\text{med}}^2} \right)^{3/2} \quad (3.6)$$

$$\Gamma_{\bar{q}q}^A = \frac{3g_q^2 M_{\text{med}}}{12\pi} \left( 1 - \frac{4m_q^2}{M_{\text{med}}^2} \right)^{3/2}. \quad (3.7)$$

Note the color factor 3 in the quark terms. Figure 3.2 shows the minimal width as a function of mediator mass for both vector and axial-vector mediators assuming couplings of 1. With this choice of the couplings, the dominant contribution to the minimal width comes from the quarks due to the color factor enhancement.

The simplified models described here have four free parameters: mediator mass  $M_{\text{med}}$ , Dark Matter mass  $m_{\text{DM}}$ , coupling of the mediator to quarks  $g_q$  and coupling of the mediator to Dark Matter  $g_{\text{DM}}$ . In order to determine an optimal choice of the parameter grid for presentation of the early Run-2 results, dependencies of the kinematic quantities and cross sections on the individual parameters need to be studied. The following paragraphs list the main observations from



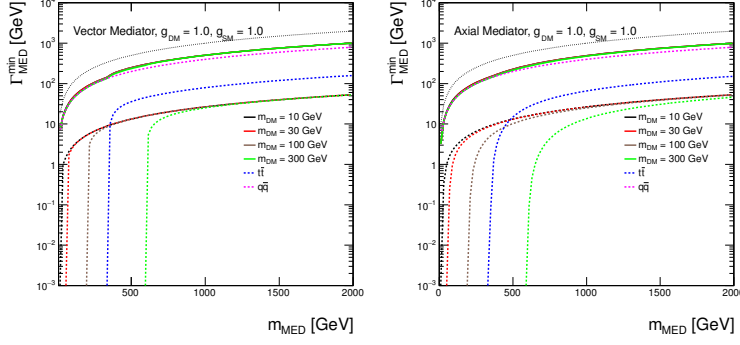


Figure 3.2: Minimal width as a function of mediator mass for vector and axial-vector mediator assuming couplings of 1. The total width is shown as solid lines for Dark Matter masses of 10 GeV, 30 GeV, 100 GeV and 300 GeV in black, red, brown and green, respectively. The individual contributions from Dark Matter are indicated by dotted lines with the same colors. The contribution from all quarks but top is shown as magenta dotted line and the contribution from top quarks only is illustrated by the dotted blue line. The dotted black line shows the extreme case  $\Gamma_{\min} = M_{\text{med}}$ .

the scans over the parameters that support the final proposal for the parameter grid.

*Scan over the couplings* Figure 3.3 reveals there are no differences in the shape of the  $\cancel{E}_T$  distribution among the samples where the pair of 10 GeV Dark Matter particles are produced on-shell from the mediator of 1 TeV, generated with different choice of the coupling strength. The considered coupling values range from 0.1 to 1.45, where the latter value approximates the maximum allowed coupling value, holding  $g_q = g_{\text{DM}}$ , such that  $\Gamma_{\min} < M_{\text{med}}$ . Based on similar plots for different choices of mediator and Dark Matter masses, it is concluded that the shapes of kinematic distributions are not altered neither for the on-shell Dark Matter production where  $M_{\text{med}} > 2m_{\text{DM}}$ , nor for the off-shell Dark Matter production where  $M_{\text{med}} < 2m_{\text{DM}}$ . Only the cross sections change. Differences in kinematic distributions are expected only close to the transition region where both on-shell and off-shell regimes mix.

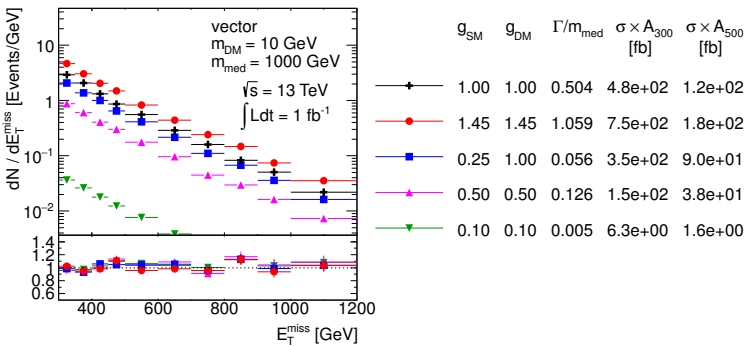


Figure 3.3: Scan over couplings. The  $\cancel{E}_T$  distribution is compared for the vector mediator models using the parameters as indicated. Ratios of the normalized distributions with respect to the first one are shown.  $A_{300}$  and  $A_{500}$  in the table denote the acceptance of the  $\cancel{E}_T > 300$  GeV and  $\cancel{E}_T > 500$  GeV cut, respectively.

The only place where special care needs to be taken are extremely heavy and narrow mediators, in other words with low couplings. Figure 3.4 suggests a change in the shape of the  $\cancel{E}_T$  distribution for 5 TeV mediator once  $\Gamma_{\min}/M_{\text{med}}$  gets down to the order of percent or

below. This, however, does not come from physics as it is a feature of the generator implementation, where a cutoff for the regions far away from the mediator mass is often used. This is illustrated in Fig. 3.5 showing the invariant mass of the Dark Matter pair in the samples generated for 7 TeV mediator with different coupling strength. In all cases, it is expected to observe a peak around the mediator mass with a tail extending to  $m_{\tilde{\chi}\chi} \rightarrow 0$ , significantly enhanced by parton distribution functions at low Bjorken  $x$ . For coupling strength 1 and 3, the massive enhancement at  $m_{\tilde{\chi}\chi} \rightarrow 0$  implies the resonant production at  $m_{\tilde{\chi}\chi} = 7 \text{ TeV}$  is statistically suppressed such that barely any events are generated there. However, for narrower mediators with couplings below 1, the peak around 7 TeV is clearly visible in the generated sample and the dominant tail at  $m_{\tilde{\chi}\chi} \rightarrow 0$  is artificially cut off, leading to unphysical cross section predictions and kinematic shapes. This explains why the sample with the narrowest mediator in Fig. 3.4 is heavily suppressed in terms of production cross section and also gives different  $\cancel{E}_T$  shape. In general, for such extreme parameter choices the EFT model should give the correct answer. In case the simplified model calculation does not reproduce the EFT result, the phase space generation of the simplified model has to be carefully examined in order to understand the cause of the problem. Fortunately, this is a rather academic discussion as such extreme corners of the parameter space are not going to be considered for presentation of Run-2 results.

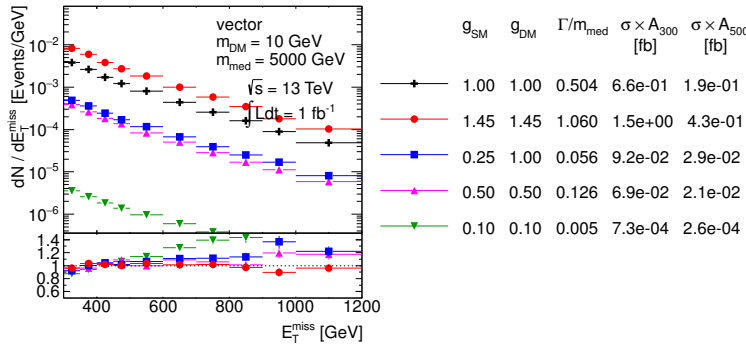


Figure 3.4: Scan over couplings. The  $\cancel{E}_T$  distribution is compared for the vector mediator models using the parameters as indicated. Ratios of the normalized distributions with respect to the first one are shown.  $A_{300}$  and  $A_{500}$  in the table denote the acceptance of the  $\cancel{E}_T > 300 \text{ GeV}$  and  $\cancel{E}_T > 500 \text{ GeV}$  cut, respectively.

*Scan over the Dark Matter mass* For the fixed mediator mass and couplings, both the cross section and the kinematic distributions remain similar for different Dark Matter masses as long as  $M_{\text{med}} > 2m_{\text{DM}}$ . This is illustrated in Fig. 3.6 on an example of 1 TeV mediator and Dark Matter masses ranging from 10 GeV to 300 GeV. It is observed that the cross section decreases as the Dark Matter mass reaches closer to  $M_{\text{med}}/2$ . Once the Dark Matter pair is produced off-line, the cross section of such simplified model is suppressed and the  $\cancel{E}_T$

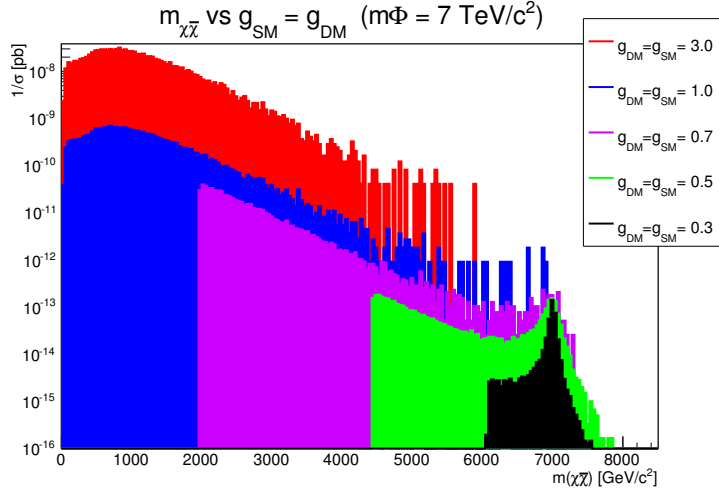


Figure 3.5: Invariant mass of the Dark Matter pair in the samples with  $M_{\text{med}} = 7 \text{ TeV}$  and different coupling strengths.

spectrum hardens, as demonstrated with the choice of 1 TeV Dark Matter in the same plot. Figure 3.7 reveals the  $\cancel{E}_T$  spectrum hardens further with increasing Dark Matter mass, accompanied by the gradual decrease of the cross section. From these observations one can conclude:

- A coarse binning along  $m_{\text{DM}}$  is sufficient at  $M_{\text{med}} \gg 2m_{\text{DM}}$ .
- Finer binning is needed in order to capture the changes in the cross section and kinematic quantities close to the production threshold on both sides around  $M_{\text{med}} = 2m_{\text{DM}}$ .
- Due to the significant cross section suppression of the off-shell Dark Matter pair production, it is not necessary to populate the parameter space  $M_{\text{med}} \ll 2m_{\text{DM}}$  since the LHC is not going to be able to probe the models there.

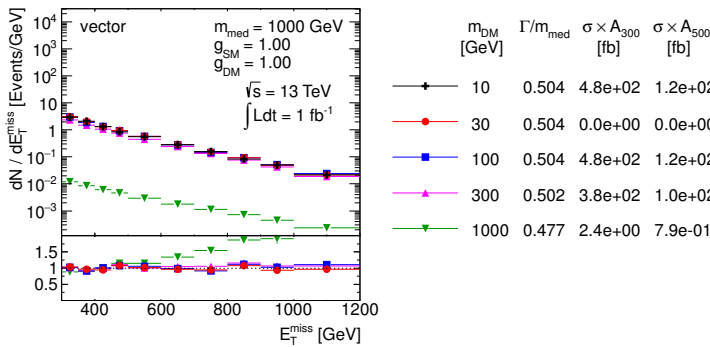


Figure 3.6: Scan over Dark Matter mass. The  $\cancel{E}_T$  distribution is compared for the vector mediator models using the parameters as indicated. Ratios of the normalized distributions with respect to the first one are shown.  $A_{300}$  and  $A_{500}$  in the table denote the acceptance of the  $\cancel{E}_T > 300 \text{ GeV}$  and  $\cancel{E}_T > 500 \text{ GeV}$  cut, respectively.

*Scan over the mediator mass* Changing the mediator mass for fixed Dark Matter mass and couplings leads to significant differences in

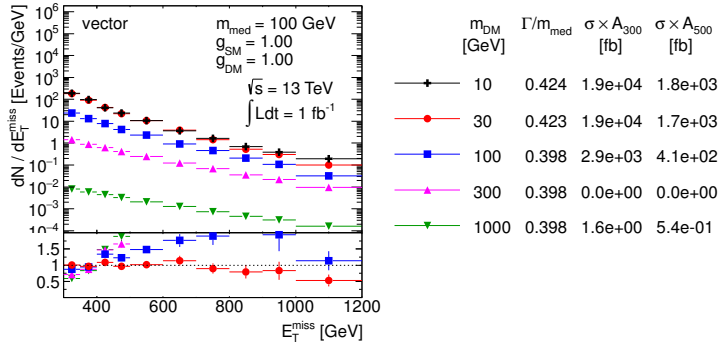


Figure 3.7: Scan over Dark Matter mass. The  $E_T$  distribution is compared for the vector mediator models using the parameters as indicated. Ratios of the normalized distributions with respect to the first one are shown.  $A_{300}$  and  $A_{500}$  in the table denote the acceptance of the  $E_T > 300$  GeV and  $E_T > 500$  GeV cut, respectively.

cross section and shapes of the kinematic variables for  $M_{\text{med}} > 2m_{\text{DM}}$  as shown in Fig. 3.8. As expected, higher mediator masses lead to harder  $E_T$  spectra. On the other hand, the  $E_T$  shapes are similar in the off-shell Dark Matter production regime as well as no dramatic differences in cross sections are observed, which is illustrated in Fig. 3.9. Therefore, a coarse binning along  $m_{\text{DM}}$  is sufficient at  $M_{\text{med}} \ll 2m_{\text{DM}}$ .

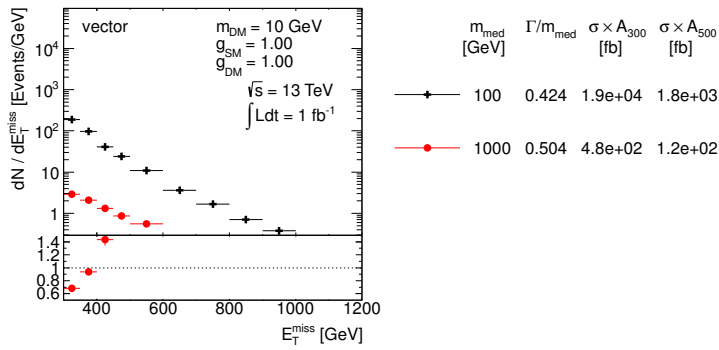


Figure 3.8: Scan over mediator mass. The  $E_T$  distribution is compared for the vector mediator models using the parameters as indicated. Ratios of the normalized distributions with respect to the first one are shown.  $A_{300}$  and  $A_{500}$  in the table denote the acceptance of the  $E_T > 300$  GeV and  $E_T > 500$  GeV cut, respectively.

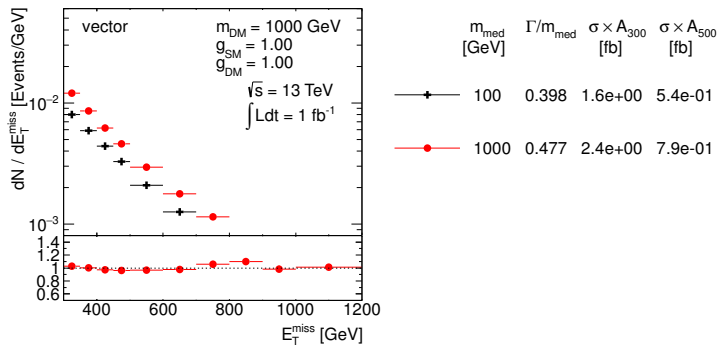


Figure 3.9: Scan over mediator mass. The  $E_T$  distribution is compared for the vector mediator models using the parameters as indicated. Ratios of the normalized distributions with respect to the first one are shown.  $A_{300}$  and  $A_{500}$  in the table denote the acceptance of the  $E_T > 300$  GeV and  $E_T > 500$  GeV cut, respectively.

*Proposed parameter grid* Based on the observations above, the following proposal is made for the presentation of the early Run-2 results

from the LHC:

(a) Give results in the  $M_{\text{med}}-m_{\text{DM}}$  plane for a particular choice of the couplings.

(b) Give results in the  $g_q-g_{\text{DM}}$  plane for a particular choice of the masses.

We choose to display the results in the  $M_{\text{med}}-m_{\text{DM}}$  plane for the choice of the couplings  $g_q = g_{\text{DM}} = 1$ . In order to motivate the highest mediator mass grid point, the expected sensitivity of Run-2 LHC data needs to be taken into account. The expected upper limit at 95% confidence level on the product of cross section, acceptance and efficiency,  $\sigma \times A \times \epsilon$ , in the final Run-1 ATLAS mono-jet analysis [A<sup>+</sup>15] is 51 fb and 7.2 fb for  $E_T > 300$  GeV and  $E_T > 500$  GeV, respectively. The ATLAS 14 TeV prospects [ATL14] predict twice better sensitivity with the first 5 fb<sup>-1</sup> of data already. Given the cross section for  $V$ +jets processes increases by roughly factor 2 when going from  $\sqrt{s} = 8$  TeV to 13 TeV, similar fiducial cross section limits can be expected with the first Run-2 data as from the final Run-1 analysis. The generator level cross section times the acceptance at  $E_T > 500$  GeV for the model with couplings  $g_q = g_{\text{DM}} = 1$ , light Dark Matter of 10 GeV and 1 TeV vector mediator is at the order of 100 fb, i.e. the early Run-2 mono-jet analysis is going to be sensitive to heavier mediators than this. The value of  $\sigma \times A$  at  $E_T > 500$  GeV for 5 TeV vector mediator is at the order of 0.1 fb, therefore this model probably lies beyond the reach of the LHC. Based on these arguments, the following  $M_{\text{med}}$  grid points are chosen, equidistant in the logarithmic scale: 10 GeV, 30 GeV, 100 GeV, 300 GeV, 1000 GeV and 3000 GeV. Given the fact that significant changes in cross section happen around the  $M_{\text{med}} = 2m_{\text{DM}}$  threshold, the  $m_{\text{DM}}$  grid points are taken at  $M_{\text{med}}/2$ , namely: 5 GeV, 15 GeV, 50 GeV, 150 GeV, 500 GeV and 1500 GeV. The detailed studies of the impact of the parameter changes on the cross section and kinematic distributions presented earlier in this section support removing some of the grid points and rely on interpolation. The optimised grids proposed for the vector and axial-vector mediators are given in Fig. 3.10, containing 24 mass points each.

The presentation of the results in the  $g_q-g_{\text{DM}}$  plane for fixed masses benefits from cross section scaling and is discussed in Section 3.3.

### 3.2 Scalar and pseudoscalar mediator, s-channel exchange

The matrix element implementation of the s-channel spin-0 mediated DM production is available in POWHEG with the full top-loop calculation at LO [HR15]. The model assumes Dirac Dark Matter particles and is based on the minimal flavor violation (MFV), which motivates

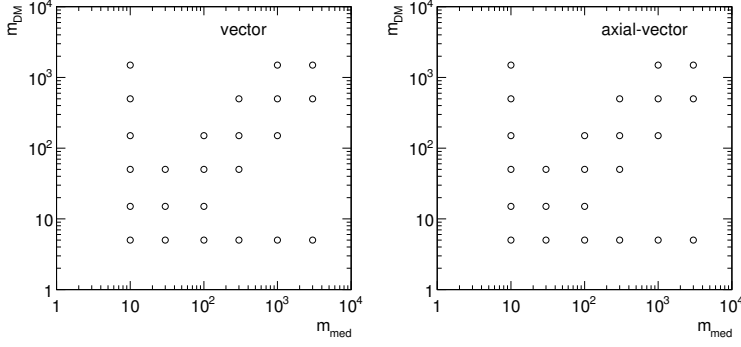


Figure 3.10: Proposed parameter grid for vector and axial-vector mediator in the  $M_{\text{med}}-m_{\text{DM}}$  plane.

Higgs-like Yukawa couplings of the mediator to the Standard Model quarks. No other couplings, such as to leptons, are allowed in this model. The following two cases are considered:

- (a) scalar couplings to DM and SM,
- (b) pseudo-scalar couplings to DM and SM

with the corresponding Lagrangians written as:

$$\mathcal{L}_{\text{scalar}} = g_q \sum \frac{m_q}{v} (\bar{q}q)S + g_{\text{DM}}(\bar{\chi}\chi)S \quad (3.8)$$

$$\mathcal{L}_{\text{pseudo-scalar}} = g_q \sum \frac{m_q}{v} (\bar{q}\gamma^5 q)P + g_{\text{DM}}(\bar{\chi}\gamma^5 \chi)P \quad (3.9)$$

$$(3.10)$$

where  $v = 246 \text{ GeV}$  denotes the Higgs vacuum expectation value.

We choose to consider minimal mediator width given by Eq. 3.3, where the individual contributions follow from

$$\Gamma_{\bar{\chi}\chi}^S = \frac{g_{\text{DM}}^2 M_{\text{med}}}{8\pi} \left(1 - \frac{4m_{\text{DM}}^2}{M_{\text{med}}^2}\right)^{3/2} \quad (3.11)$$

$$\Gamma_{\bar{q}q}^S = \frac{3g_q^2 M_{\text{med}}}{8\pi} \frac{m_q^2}{v^2} \left(1 - \frac{4m_q^2}{M_{\text{med}}^2}\right)^{3/2} \quad (3.12)$$

$$\Gamma_{\bar{\chi}\chi}^P = \frac{g_{\text{DM}}^2 M_{\text{med}}}{8\pi} \sqrt{1 - \frac{4m_{\text{DM}}^2}{M_{\text{med}}^2}} \quad (3.13)$$

$$\Gamma_{\bar{q}q}^P = \frac{3g_q^2 M_{\text{med}}}{8\pi} \frac{m_q^2}{v^2} \sqrt{1 - \frac{4m_q^2}{M_{\text{med}}^2}}. \quad (3.14)$$

The minimal width for scalar and pseudo-scalar mediators with  $g_q = g_{\text{DM}} = 1$  are shown in Fig. 3.11, illustrating the effect of the Higgs-like Yukawa couplings. For the mediator masses above twice the top quark mass  $m_t$ , the minimal width receives the dominant contribution from the top quark. For lighter mediator masses, Dark Matter dominates as the couplings to lighter quarks are Yukawa suppressed. Note that we decide to ignore the partial width coming from gluons through loops as it can be safely neglected [HR15].

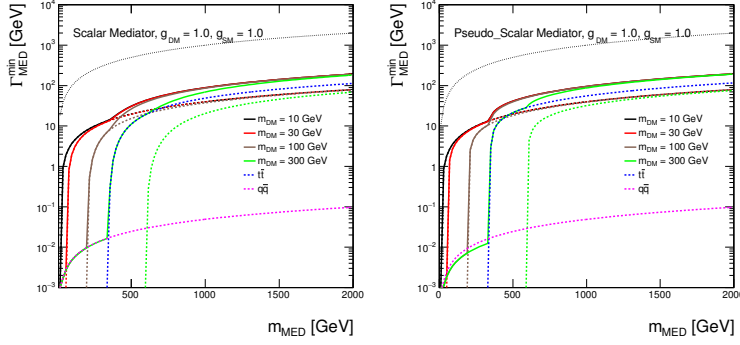


Figure 3.11: Minimal width as a function of mediator mass for scalar and pseudo-scalar mediator assuming couplings of 1. The total width is shown as solid lines for Dark Matter masses of 10 GeV, 30 GeV, 100 GeV and 300 GeV in black, red, brown and green, respectively. The individual contributions from Dark Matter are indicated by dotted lines with the same colors. The contribution from all quarks but top is shown as magenta dotted line and the contribution from top quarks only is illustrated by the dotted blue line. The dotted black line shows the extreme case  $\Gamma_{\min} = M_{\text{med}}$ .

Similarly as in the case of the vector and axial-vector mediators, scans in the parameter space are performed also for the scalar and pseudo-scalar mediators in order to decide on the optimised parameter grid for the presentation of Run-2 results. Figures ?? show the scans over the couplings, Dark Matter mass and mediator mass and the same conclusions apply as in Section 3.1.

Since the top quark gives the dominant contribution to the mediator width due to Higgs-like Yukawa couplings, the effect of the top channel opening in the mediator production was studied in addition. Scan over the mediator mass is shown in Fig. 3.16 where the mediator masses 300 GeV and 500 GeV are chosen to be below and above  $2m_t$ . The off-shell Dark Matter production regime is assumed by taking  $m_{\text{DM}} = 1$  TeV in order to allow studying solely the effects of the couplings to quarks. No differences in the kinematic distributions are observed and also the cross sections remain similar in this case. Therefore, it is concluded that no significant changes appear for mediator masses around the  $2m_t$  threshold.

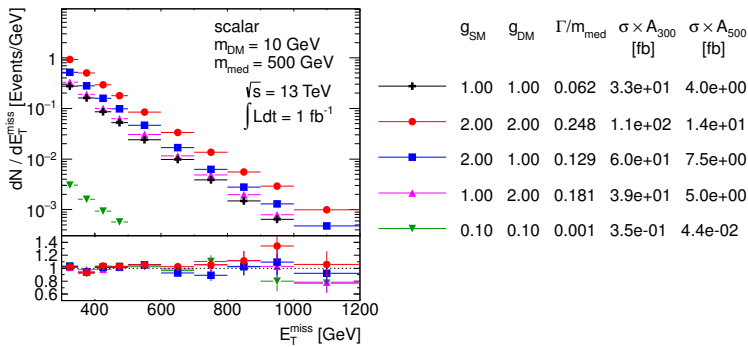


Figure 3.12: Scan over couplings. The  $E_T$  distribution is compared for the scalar mediator models using the parameters as indicated. Ratios of the normalized distributions with respect to the first one are shown.  $A_{300}$  and  $A_{500}$  in the table denote the acceptance of the  $E_T > 300$  GeV and  $E_T > 500$  GeV cut, respectively.

The optimized parameter grid in the  $M_{\text{med}}-m_{\text{DM}}$  plane for scalar and pseudo-scalar mediators is motivated by similar arguments as in the previous section. Therefore, similar pattern is followed here, taking again  $g_q = g_{\text{DM}} = 1$ . Only the sensitivity to the highest me-

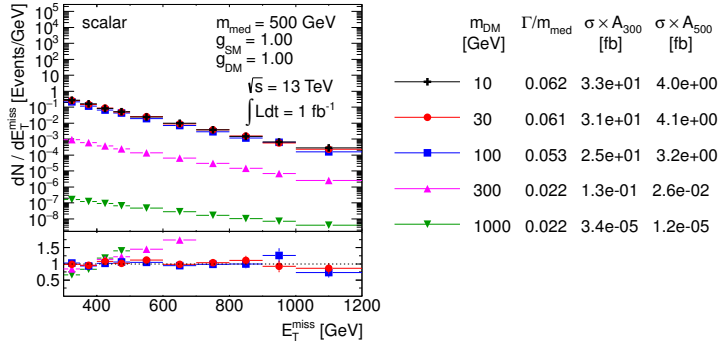


Figure 3.13: Scan over Dark Matter mass. The  $E_T$  distribution is compared for the scalar mediator models using the parameters as indicated. Ratios of the normalized distributions with respect to the first one are shown.  $A_{300}$  and  $A_{500}$  in the table denote the acceptance of the  $E_T > 300$  GeV and  $E_T > 500$  GeV cut, respectively.

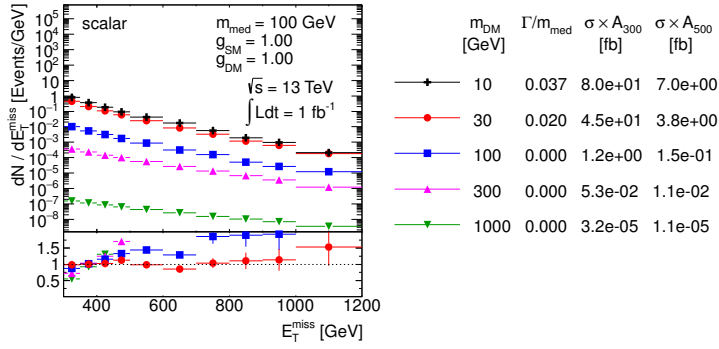


Figure 3.14: Scan over Dark Matter mass. The  $E_T$  distribution is compared for the scalar mediator models using the parameters as indicated. Ratios of the normalized distributions with respect to the first one are shown.  $A_{300}$  and  $A_{500}$  in the table denote the acceptance of the  $E_T > 300$  GeV and  $E_T > 500$  GeV cut, respectively.

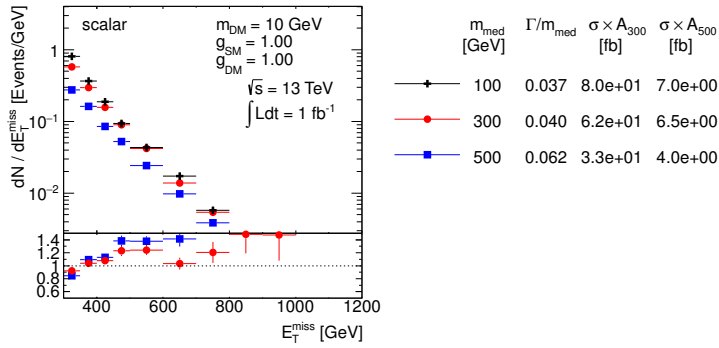


Figure 3.15: Scan over mediator mass. The  $E_T$  distribution is compared for the scalar mediator models using the parameters as indicated. Ratios of the normalized distributions with respect to the first one are shown.  $A_{300}$  and  $A_{500}$  in the table denote the acceptance of the  $E_T > 300$  GeV and  $E_T > 500$  GeV cut, respectively.

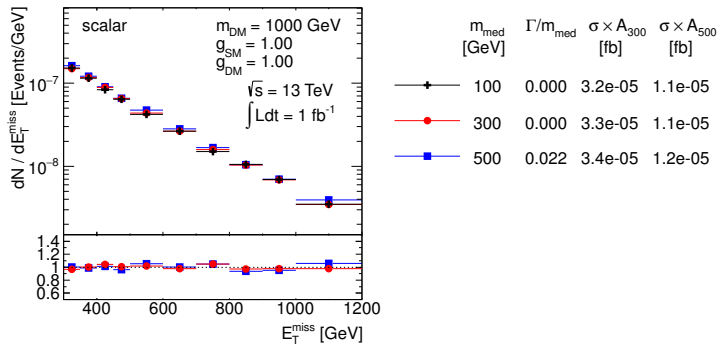


Figure 3.16: Scan over mediator mass. The  $E_T$  distribution is compared for the scalar mediator models using the parameters as indicated. Ratios of the normalized distributions with respect to the first one are shown.  $A_{300}$  and  $A_{500}$  in the table denote the acceptance of the  $E_T > 300$  GeV and  $E_T > 500$  GeV cut, respectively.



diator masses has to be revisited. The generator level cross section times the acceptance at  $\cancel{E}_T > 500$  GeV for the model with couplings  $g_q = g_{\text{DM}} = 1$ , light Dark Matter of 10 GeV and 500 GeV scalar mediator is at the order of 10 fb, i.e. just at the edge of the early Run-2 sensitivity. Increasing the mediator mass to 1 TeV pushes the product  $\sigma \times A$  down to approximately 0.1 fb, beyond the LHC sensitivity. Therefore, we choose to remove the 3 TeV mediator mass from the grid and present the final grid with 19 mass points only in Fig. 3.17.

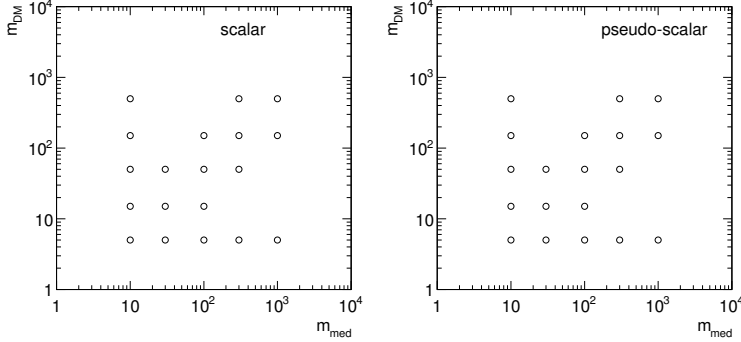


Figure 3.17: Proposed parameter grid for scalar and pseudo-scalar mediator in the  $M_{\text{med}}-m_{\text{DM}}$  plane.

The proposal for the scan in the  $g_q$ - $g_{\text{DM}}$  plane is described in the following section.

### 3.3 Cross section scaling

The aim of the parameter grid optimization is to find out whether certain parts of the parameter space can be omitted and one can rely on the neighboring grid points in order to populate the missing parts. There are two ways of doing this:

- Interpolation is used in-between the grid points that are close enough such that finer granularity is not needed for the presentation purposes, or between the points where smooth or no changes of the results are expected. The latter argument is exactly the one that motivates the reduction of the grid points in the  $M_{\text{med}}-m_{\text{DM}}$  plane.
- Recalculation of the results can be used when the dependencies with respect to the neighboring grid points are known.

The results of the scan over the couplings presented in the previous sections indicate there are no changes in kinematic distributions for different choices of the coupling strengths. This means that the acceptance remains the same in the whole  $g_q$ - $g_{\text{DM}}$  plane and it is sufficient to perform the detector simulation only for one single grid point. The resulting truth-level selection acceptance and the detector

reconstruction efficiency can then be applied to all remaining grid points in the  $g_q$ - $g_{\text{DM}}$  plane where only the generator-level cross section needs to be known. This significantly reduces the computing time as the detector response is by far the most expensive part of the Monte Carlo sample production. However, a further step can be taken if a parameterization of the cross section dependence from one grid point to another exists, in which case the number of generated samples can be reduced even further.

Let us now elaborate on a cross section scaling procedure. The propagator on the s-channel exchange is written in a Breit-Wigner form as  $\frac{1}{\sqrt{s}-M_{\text{med}}^2+iM_{\text{med}}\Gamma}$ . The relative size of the center-of-mass energy defined by the two partons entering the hard process and the mediator mass allows to classify the production in the following way:

- off-shell production when  $\sqrt{s} \gg M_{\text{med}}$  leading to suppressed cross sections,
- on-shell production when  $\sqrt{s} \sim M_{\text{med}}$  leading to enhanced cross sections,
- effective field theory (EFT) limit when  $\sqrt{s} \ll M_{\text{med}}$ .

All three categories can be distinguished in Fig. 3.18 showing the upper limit on the interaction scale  $M^* \equiv M_{\text{med}}/\sqrt{g_q g_{\text{DM}}}$  for vector mediator. In the case of the off-shell production and the EFT limit, the first term in the propagator dominates which reduces the dependence on the mediator width. Therefore, in these cases one can approximate the cross section as

$$\sigma \propto g_q^2 g_{\text{DM}}^2. \quad (3.15)$$

The on-shell production regime is the most interesting one as it gives the best chances for a discovery at the LHC given the cross section enhancement. The propagator term with the width cannot be neglected in this case and, in the narrow width approximation, one can integrate

$$\int \frac{ds}{(s-M_{\text{med}}^2)^2 + M_{\text{med}}^2 \Gamma^2} = \frac{\pi}{M_{\text{med}} \Gamma} \quad (3.16)$$

which further implies the cross section scaling

$$\sigma \propto \frac{g_q^2 g_{\text{DM}}^2}{\Gamma}. \quad (3.17)$$

Since  $\Gamma \sim g_q^2 + g_{\text{DM}}^2$ , one can simplify this rule in the extreme cases as follows

$$\sigma \propto \frac{g_q^2 g_{\text{DM}}^2}{g_q^2 + g_{\text{DM}}^2} \xrightarrow{g_q \ll g_{\text{DM}}} g_q^2 \quad (3.18)$$

$$\sigma \propto \frac{g_q^2 g_{\text{DM}}^2}{g_q^2 + g_{\text{DM}}^2} \xrightarrow{g_q \gg g_{\text{DM}}} g_{\text{DM}}^2. \quad (3.19)$$

However, it is important to keep in mind that there is no simple scaling rule for how the cross section changes with the Dark Matter mass, mediator mass and the mediator width because PDFs matter in such cases as well. Therefore, the scaling procedure outlined above is expected to work only for fixed masses and fixed mediator width.

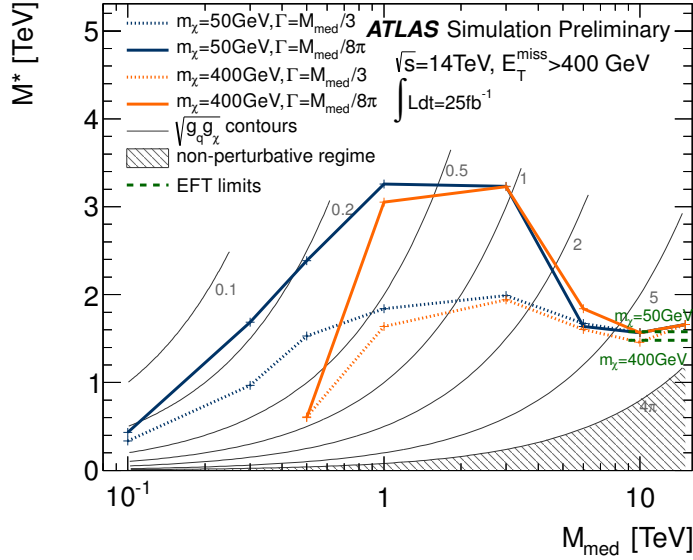


Figure 3.18: Comparison of the 95% CL lower limits on the scale of the interaction of a  $Z'$ -like simplified model at 14 TeV, in terms of the mediator mass. Corresponding limits from EFT models are shown on the same plot as green dashed lines to show equivalence between the two models for high mediator masses. Taken from Ref. [ATL14].

Figures 3.19 and 3.20 show the minimal width in the  $g_q$ - $g_{DM}$  plane for all vector, axial-vector, scalar and pseudo-scalar mediators for  $M_{med} = 100$  GeV and 1000 GeV, respectively, taking  $m_{DM} = 10$  GeV. The individual colors indicate the lines of constant width along which the cross section scaling works. For vector and axial-vector mediators, the minimal width is predominantly defined by  $g_q$  due to the number of quark flavors and the color factor. On the contrary, both the Standard Model and Dark Matter partial width have comparable contributions in case of scalar and pseudo-scalar mediators if the top quark channel is open ( $M_{med} > 2m_t$ ). However, mostly  $g_{DM}$  defines the minimal width for  $M_{med} < 2m_t$  due to the Yukawa-suppressed light quark couplings.

The performance of the cross section scaling is demonstrated in Fig. 3.21 where the mass point  $M_{med} = 1$  TeV and  $m_{DM} = 10$  GeV is chosen and rescaled from the starting point  $g_q = g_{DM} = 1$  according to Eq. 3.17 to populate the whole  $g_q$ - $g_{DM}$  plane. This means the width is not kept constant in this test and this is done in purpose in order to point out deviations from the scaling when the width is altered. For each mass point, the rescaled cross section is compared to the generator cross section and the ratio of the two is plotted. For the given choice of the mass points, the scaling seems to work

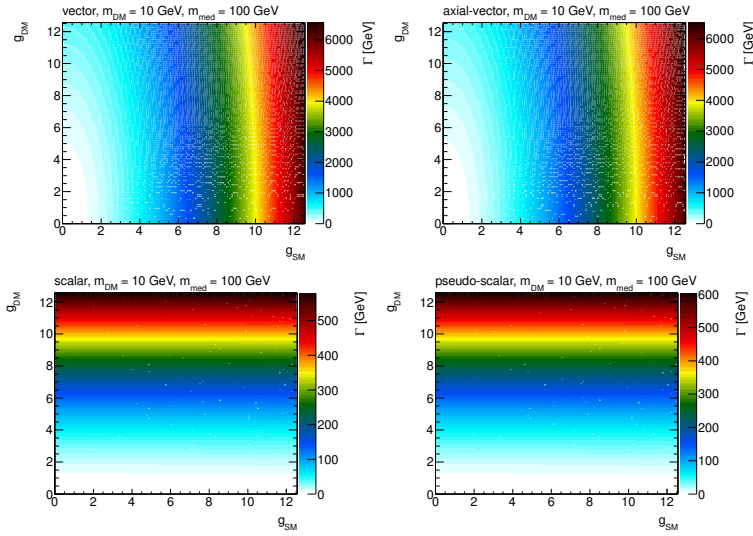


Figure 3.19: Minimal width for vector, axial-vector, scalar and pseudo-scalar mediators as a function of the individual couplings  $g_q$  and  $g_{DM}$ , assuming  $M_{med} = 100 \text{ GeV}$  and  $m_{DM} = 10 \text{ GeV}$ .

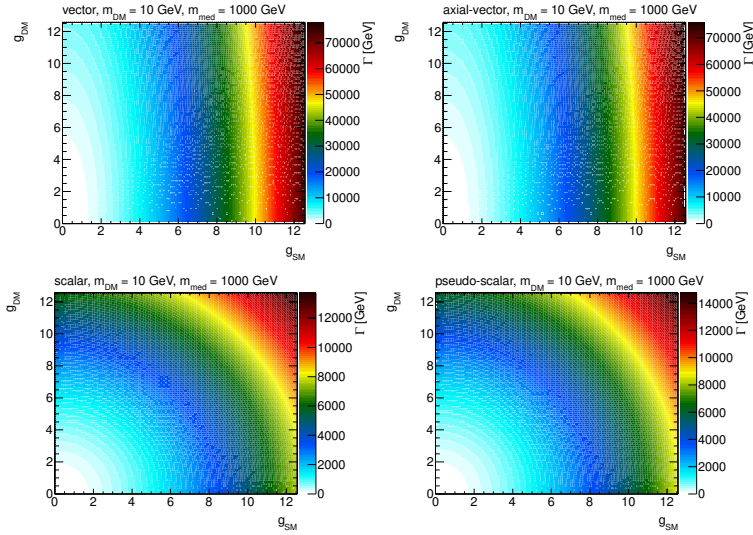


Figure 3.20: Minimal width for vector, axial-vector, scalar and pseudo-scalar mediators as a function of the individual couplings  $g_q$  and  $g_{DM}$ , assuming  $M_{med} = 1 \text{ TeV}$  and  $m_{DM} = 10 \text{ GeV}$ .

approximately with the precision of  $\sim 20\%$  in the region where  $\Gamma_{\min} < M_{\text{med}}$ . Constant colors indicate the lines along which the cross section scaling works precisely and there is a remarkable resemblance of the patterns shown in the plots of the mediator width. To prove the scaling along the lines of constant width works, one such line is chosen in Fig. 3.22 for a scalar mediator, defined by  $M_{\text{med}} = 300 \text{ GeV}$ ,  $m_{\text{DM}} = 100 \text{ GeV}$ ,  $g_q = g_{\text{DM}} = 1$ , and the rescaled and generated cross sections are found to agree within 3%.

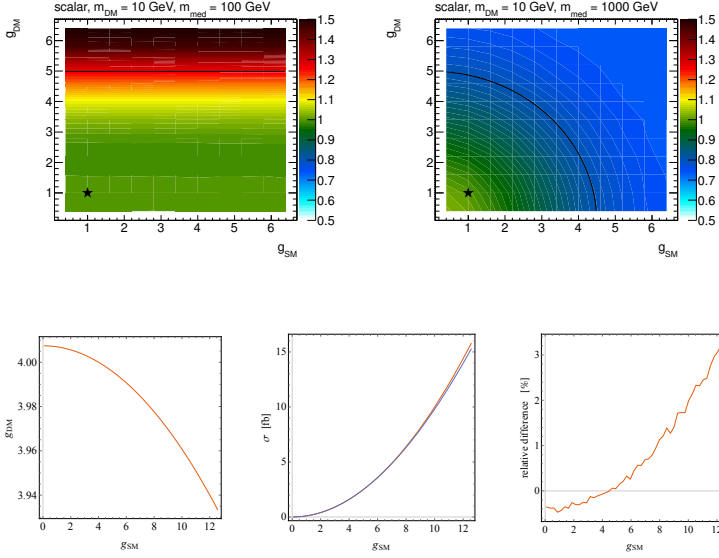


Figure 3.21: Ratio of the rescaled and generated cross sections in the  $g_q$ - $g_{\text{DM}}$  plane. The point at  $g_q = g_{\text{DM}} = 1$ , taken as a reference for the rescaling, is denoted by a star symbol. Scalar model with  $M_{\text{med}} = 100 \text{ GeV}$  (left) and  $1 \text{ TeV}$  (right) is plotted for  $m_{\text{DM}} = 10 \text{ GeV}$ . The limiting case  $\Gamma_{\min} = M_{\text{med}}$  is shown as a black line.

Figure 3.22: Scaling along the lines of constant width. The line of constant width for  $M_{\text{med}} = 300 \text{ GeV}$  and  $m_{\text{DM}} = 100 \text{ GeV}$ , intercepting  $g_q = g_{\text{DM}} = 4$  is shown on left. The generated and rescaled cross sections are compared in the middle, the corresponding ratio is shown on right.

*Proposed parameter grid* We propose to present the results in the  $g_q$ - $g_{\text{DM}}$  plane using the following prescription:

- Since the shapes of kinematic quantities do not change for different couplings, use the acceptance and efficiency for the available  $m_{\text{DM}} = 50 \text{ GeV}$ ,  $M_{\text{med}} = 300 \text{ GeV}$ ,  $g_q = g_{\text{DM}} = 1$  grid point from the  $M_{\text{med}}-m_{\text{DM}}$  plane for the scalar and pseudo-scalar mediator. In case of the vector and axial-vector mediator, use the grid point  $m_{\text{DM}} = 50 \text{ GeV}$ ,  $M_{\text{med}} = 1 \text{ TeV}$ ,  $g_q = g_{\text{DM}} = 1$ .
- Generate additional samples in order to get generator cross sections only. For scalar and pseudo-scalar mediator, choose  $m_{\text{DM}} = 50 \text{ GeV}$ ,  $M_{\text{med}} = 300 \text{ GeV}$  with the following values for  $g_q = g_{\text{DM}}$ : 0.1, 2, 3, 4, 5, 6. For vector and axial vector mediator, choose  $m_{\text{DM}} = 50 \text{ GeV}$ ,  $M_{\text{med}} = 1 \text{ TeV}$  with the following values for  $g_q = g_{\text{DM}}$ : 0.1, 0.25, 0.5, 0.75, 1.25, 1.5. The upper values are defined by the minimal width reaching the mediator mass.
- Rescale the generator cross sections along the lines of constant width in order to populate the whole  $g_q$ - $g_{\text{DM}}$  plane.

*Rescaling to different mediator width* In general there may be an interest to consider larger mediator masses than  $\Gamma_{\min}$  in order to accommodate further couplings of the mediator. The cross section scaling method described above can be used to reinterpret the results presented for the minimal width, since multiplying the width by factor  $n$  is equivalent to changing the coupling strength by factor  $\sqrt{n}$ , i.e.

$$\sigma(g_q, g_{\text{DM}}, n\Gamma_{\min}(g_q, g_{\text{DM}})) \propto \frac{g_q^2 g_{\text{DM}}^2}{\Gamma_{\min}(\sqrt{n}g_q, \sqrt{n}g_{\text{DM}})} . \quad (3.20)$$

The cross section for the sample with couplings  $g_q$  and  $g_{\text{DM}}$  and modified mediator width  $\Gamma = n\Gamma_{\min}$  can therefore be rescaled from a sample generated with the minimal width corresponding to the couplings scaled by  $\sqrt{n}$  as described in the following formula.

$$\sigma(g_q, g_{\text{DM}}, n\Gamma_{\min}(g_q, g_{\text{DM}})) = \frac{1}{n^2} \sigma(\sqrt{n}g_q, \sqrt{n}g_{\text{DM}}, \Gamma_{\min}(\sqrt{n}g_q, \sqrt{n}g_{\text{DM}})) \quad (3.21)$$

Advantage of doing this is again in the fact that no event selection and detector response needs to be simulated since the changes in couplings do not have an effect on the shapes of kinematic distributions.

### 3.3.1 POWHEG settings

This section describes specif settings for the Dark Matter models needed to run the POWHEG generation.

- The POWHEG implementation allows to generate a single sample that provides sufficient statistics in all mono-jet analysis signal regions. POWHEG generates weighted events and the bornsupfact parameter is used to set the event suppression factor according to

$$F(k_T) = \frac{k_T^2}{k_T^2 + \text{bornsupfact}^2} . \quad (3.22)$$

In this way, the events at low  $\cancel{E}_T$  are suppressed and receive higher event weights which ensures higher statistics at high  $\cancel{E}_T$ . We recommend to set bornsupfact to 1000.

- The bornktmin parameter allows to suppress the low  $\cancel{E}_T$  region even further by starting the generation at a certain value of  $k_T$ . It is recommended to set this parameter to half the lower analysis  $\cancel{E}_T$  cut, therefore the proposed value for bornktmin is 150.
- Set runningwidth to 0.
- Set mass\_low and mass\_high to -1.

- The minimal values for `ncall1`, `itmx1`, `ncall2`, `itmx2` are 250000, 5, 1000000, 5 for the DMV model, respectively. In order to increase speed, set `foldsci` and `foldy` to 2 and keep `foldphi` at 1.
- The minimal values for `ncall1`, `itmx1`, `ncall2`, `itmx2` are 100000, 5, 100000, 5 for the DMS\_tloop model, respectively.
- Allow negative weights for the DMV model by setting `withnegweights` to 1.
- Since the DMS\_tloop model is a leading order process, set `L0events` and `bornonly` are set to 1 internally.

### 3.4 Colored scalar mediator, $t$ -channel exchange

An alternative set of simplified models exist where the mediator is exchanged in the  $t$ -channel, thereby coupling the quark and dark matter particle directly. Under the assumption that  $\chi$  is a Standard Model (SM) singlet, the mediating particle, labeled  $\phi$ , is necessarily charged and coloured. This model is parallel to, and partially motivated by, the squark of the MSSM, but in this case the  $\chi$  is chosen to be Dirac. Following the example of Ref. [PVZ14], the interaction Lagrangian is written as

$$\mathcal{L}_{\text{int}} = g \sum_{i=1,2,3} (\phi_L^i \bar{Q}_L^i + \phi_{uR}^i \bar{u}_R^i + \phi_{dR}^i \bar{d}_R^i) \chi \quad (3.23)$$

(Note: [PVZ14] uses only  $i = 1, 2$ , but I think it's fine to extend this to 3 here.) where  $Q_L^i$ ,  $u_R^i$  and  $d_R^i$  are the SM quarks and  $\phi_L^i$ ,  $\phi_{uR}^i$  and  $\phi_{dR}^i$  are the corresponding mediators, which (unlike the  $s$ -channel mediators) must be heavier than  $\chi$ . These mediators have SM gauge representations under  $(SU(3), SU(2))_Y$  of  $(3, 2)_{-1/6}$ ,  $(3, 1)_{2/3}$  and  $(3, 1)_{-1/3}$  respectively. Variations of the model previously studied include coupling to the left-handed quarks only [CEHL14, BDS<sup>+</sup>14], to the  $\phi_{uR}^i$  [DNRT13] or  $\phi_{dR}^i$  [PVZ14, A<sup>+</sup>14b], or some combination [BB13, AWZ14].

Minimal Flavour Violation (MFV) requires that the mediator masses for each flavour be equal; the same logic also applies to the couplings  $g$ . The available parameters are then

$$\{m_\chi, M_\phi, g\}. \quad (3.24)$$

In practice, the third mediator mass and coupling could be separated from the other two, if higher order corrections to the MFV prediction arise due to the large top Yukawa coupling – a common

variation is then to define this split between the first two generations  
and the third, so the parameters are extended to

$$\{m_\chi, M_{\phi_{1,2}}, M_{\phi_3}, g_{1,2}, g_3\}. \quad (3.25)$$

The width of each mediator is expressed, using the example of  
decay to an up quark, as

$$\begin{aligned} \Gamma(\phi_i \rightarrow \bar{u}_i \chi) &= \frac{g_i^2}{16\pi M_{\phi_i}^3} (M_{\phi_i}^2 - m_{u_i}^2 - m_\chi^2) \\ &\times \sqrt{M_{\phi_i}^4 + m_{u_i}^4 + m_\chi^4 - 2M_{\phi_i}^2 m_{u_i}^2 - 2M_{\phi_i}^2 m_\chi^2 - 2m_{u_i}^2 m_\chi^2}, \end{aligned} \quad (3.26)$$

this reduces to

$$\frac{g_i^2 M_{\phi_i}}{16\pi} \left(1 - \frac{m_\chi^2}{M_{\phi_i}^2}\right)^2 \quad (3.27)$$

in the limit  $M_{\phi_i}, m_\chi \gg m_{u_i}$ .

An interesting point of difference with the  $s$ -channel simplified  
models is that the mediator can radiate a SM object, such as a jet or  
gauge boson, thus providing three separate mono- $X$  diagrams which  
must be considered together in calculations. This model can also  
give a signal in the di-jet + MET channel when, for example, the  $\chi$  is  
exchanged in the  $t$ -channel and the resulting  $\phi$  pair each decay to a  
jet +  $\chi$ .



# 4

## *Specific models for signatures with EW bosons*

In this Section, we consider models with a photon, a W boson, a Z boson or a Higgs boson in the final state, accompanied by Dark Matter particles that either couple directly to the boson or are mediated by a new particle. The experimental signature is identified as  $V+MET$ .

These models are interesting both as extensions of models where the gluon provides the experimentally detectable signature, and as stand-alone models with final states that cannot be generated by the models in Section 3.

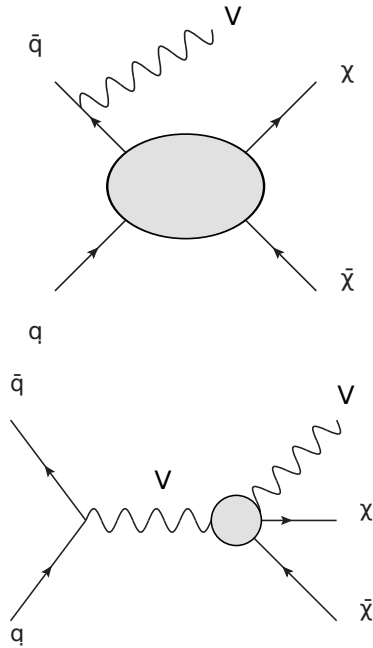


Figure 4.1: Sketch of benchmark models including a contact interaction for  $V+MET$  searches, adapted from [NCC<sup>+</sup>14].

The models considered can be divided in three categories:

*Models including a contact operator, where the boson is radiated from the initial state*

As depicted in the top diagram of Figure 4.1, these models follow the nomenclature and theory for the EFT benchmarks commonly

used by MET+X searches [GIR<sup>+</sup>10]. These models have been used in past experimental searches [Kha14, Aad14b, K<sup>+</sup>14, Aad14b, A<sup>+</sup>14a, Aad14a], and they will not be described here.

*Models including a contact operator, where the boson is directly coupled to DM*

Shown in the bottom of Figure 4.1, these models allow for a contact interaction vertex that directly couples the boson to Dark Matter.

*Simplified models where the boson is radiated from the initial state* These models follow those already described in Section 3, replacing the initial state gluon with a boson.

*V-specific simplified models* These models postulate direct couplings of new mediators to bosons, e.g. they couple the Higgs boson to a new scalar [CDM<sup>+</sup>14].

The following Sections describe the models within these categories, the parameters for each of the benchmark models chosen, the studies towards the choices of the parameters to be scanned, and finally point to the location of their Matrix Element implementation.

#### 4.1 Simplified models with ISR boson radiation

Searches in the jet+MET final state are generally more sensitive with respect to final states including bosons, due to the much larger rates of signal events featuring quark or gluon radiation with respect to radiation of bosons [ZBW13], in combination with the low branching ratios if leptons from boson decays are required in the final state. The rates for the Higgs boson radiation is too low for these models to be considered a viable benchmark [CDM<sup>+</sup>14]. However, the presence of photons leptons from W and Z decays and W or Z bosons decaying hadronically allows to reject the background more effectively, making Z/gamma/W+MET searches still worth comparing with searches in the jet+MET final state.

##### 4.1.1 Vector mediator exchanged in the s-channel

The case for searches with W bosons in the final state has so far been strengthened by the presence of particular choices of couplings between the WIMP and the up and down quarks which enhance W radiation [BT13], in the case of the exchange of a vector mediator in the s-channel. Run-1 searches have considered three sample cases for the product of up and down quark couplings to the mediator  $\xi$ :

- No couplings between mediator and either up or down quarks ( $\xi = 0$ );

- Same coupling between mediator and each of the quark types ( $\xi = 1$ );
- Coupling of opposite sign between mediator and each of the quark types ( $\xi = -1$ ).

The  $\xi = -1$  case leads to a large increase in the cross-section of the process, and modifies the spectrum of missing transverse energy or transverse mass used for the searches. The sensitivity of the W+MET search for this benchmark in this case surpasses that of the jet+MET search. However, as shown in Ref. [BCD<sup>+</sup>15], the cross-section increase is due to the production of longitudinally polarized W bosons, as a consequence of a violation of electroweak gauge symmetries. Unless further particles are introduced (in a fashion similar to the Higgs boson in the Standard Model), choosing a value of  $\xi = -1$  for this simplified model will lead to a manifest violation of unitarity at LHC energies. The simplified model with a vector mediator exchanged in the s-channel model can still be considered as a benchmark for searches with a W boson if  $\xi = 1$ . We leave the study of further models with cross-section enhancements due to different couplings to up and down quarks for studies beyond the early LHC searches covered in this document. An example of such model is the case of both DM and SM Higgs charged under a new  $U(1)'$ , with a small mass mixing between SM Z-boson and the new Zprime. This leads to different effective DM couplings to  $u_L$  and  $d_L$ , proportional to their coupling to the Z boson, detailed in Appendix B.

The scan in the parameters that characterize this simplified model for EW boson + MET searches follow what already detailed in Section 3.

As in the case of the jet+MET models, the width does not have a significant impact on the kinematic distributions relevant for those searches. An example of the particle-level analysis acceptance using the generator-level cuts from Ref. [Aad15] for the photon+MET analysis, but raising the photon  $p_T$  cut to 150 GeV is shown in Figure 4.2, comparing a width that is set to  $\Gamma = M_{med}/3$  to the minimal width (the ratio between the two widths ranges from 1.05 to 1.5 with increasing mediator masses).

Examples of relevant kinematic distributions for selected benchmark points are shown in Fig. 4.7; leading-order cross-sections for the chosen benchmark points are shown in Table ?? [TODO: Insert table of cross-sections].

#### 4.1.2 Colored scalar mediator exchanged in the s-channel

t-channel colored scalar, to be completed...

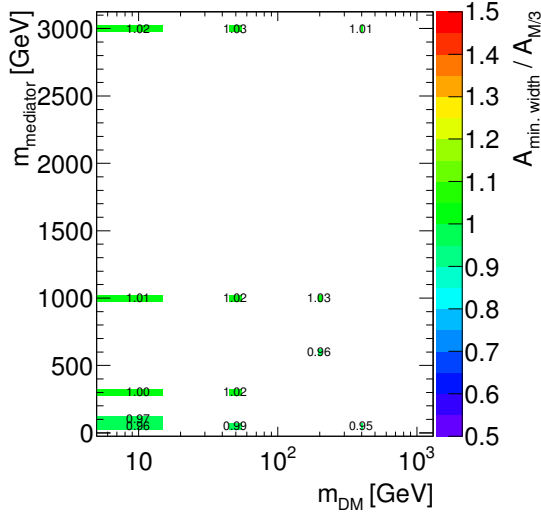


Figure 4.2: Analysis acceptance for the photon+MET analysis when varying the mediator width, in the case of a vector mediator exchanged in the  $s$ -channel

## MODEL IMPLEMENTATION

These models are generated at leading order with MadGraph 2.2.2, and parameter cards can be found on SVN [TODO: Add SVN location]. The parton shower is done using Pythia 8, with a matching scale of... [TODO: To be completed.]

### 4.2 EFT models with direct DM-boson couplings

[Linda Carpenter and Uli Haisch are rewriting this section. Changes expected:

- change of normalization and Lagrangians to be consistent with [CHH15], linked to notation of [CNS<sup>+</sup>13]
- description of dimension-5 EFTs
- addition of a dimension-5 simplified model]

A complete list of effective operators with direct DM/boson couplings for Dirac DM, up to dimension 7, can be found in [CHLR13].

Following the notation of [CNS<sup>+</sup>13], the dimension 5 benchmark models from this category have a Lagrangian that includes terms such as:

$$\frac{m_W^2}{\Lambda_5^3} \bar{\chi} \chi W^{+\mu} W_\mu^- + \frac{m_Z^2}{2\Lambda_5^3} \bar{\chi} \chi Z^\mu Z_\mu . \quad (4.1)$$

where  $m_Z$  and  $m_W$  are the masses of the Z and W boson,  $W^\mu$  and  $Z^\mu$  are the fields of the gauge bosons,  $\chi$  denote the Dark Matter fields



strengths of the SM  $U(1)$  and  $SU(2)$  gauge groups and  $\tilde{F}_i^{\mu\nu}$  their dual tensors). The Lagrangian for the scalar coupling of DM and bosons include terms such as the following:

$$\frac{1}{\Lambda_{7,S}^3} \bar{\chi}\chi \sum_i k_i F_i^{\mu\nu} F_{\mu\nu}^i + \frac{1}{\Lambda_{7,S}^3} \bar{\chi}\chi \sum_i k_i F_i^{\mu\nu} \tilde{F}_{\mu\nu}^i \quad (4.2)$$

The Lagrangian with pseudoscalar coupling includes the following terms:

$$\frac{1}{\Lambda_{7,PS}^3} \bar{\chi}\gamma^5\chi \sum_i k_i F_i^{\mu\nu} F_{\mu\nu}^i + \frac{1}{\Lambda_{7,PS}^3} \bar{\chi}\gamma^5\chi \sum_i k_i F_i^{\mu\nu} \tilde{F}_{\mu\nu}^i \quad (4.3)$$

The cut-off scales  $\Lambda$  for the separate terms can be related to operators with different Lorentz structure from Ref. [CHLR13]. Given that they do not lead to substantial differences for collider searches as shown in Figure 2 of Ref. [CNS<sup>+</sup>13], they have been denoted as  $\Lambda_{7,S}$  for the scalar case and  $\Lambda_{7,PS}$  for the pseudoscalar case.

The  $k_i$  coefficients for the dimension 7 models are related to the couplings of DM to pairs of gauge bosons by gauge invariance:

$$g_{WW} = \frac{2k_2}{s_w^2 \Lambda_7^3} \quad (4.4)$$

$$g_{ZZ} = \frac{1}{4s_w^2 \Lambda_7^3} \left( \frac{k_1 s_w^2}{c_w^2} + \frac{k_2 c_w^2}{s_w^2} \right) \quad (4.5)$$

$$g_{\gamma\gamma} = \frac{1}{4c_w^2} \frac{k_1 + k_2}{\Lambda_7^3} \quad (4.6)$$

$$g_{Z\gamma} = \frac{1}{2s_w c_w \Lambda_7^3} \left( \frac{k_2}{s_w^2} - \frac{k_1}{c_w^2} \right) \quad (4.7)$$

where  $s_w$  and  $c_w$  are respectively the sine and cosine of the weak mixing angle.

The coefficients  $k_i$  determine the relative importance of each of the boson channels, and their correlations. For example, for what concerns searches with  $W$ ,  $Z$  and photons:

- $k_2$  alone controls the rate of the coupling to  $W$  boson pairs;
- If  $k_1 = k_2$  contributions from both  $Z$  and  $\gamma$  exchange appear;
- If  $k_1 = c_w^2/s_w^2 k_2$  the  $\gamma$  exchange is negligible.

The coefficients  $k_1$  and  $k_2$  are related to the coefficients  $c_1$  and  $c_2$  in the equivalent models of Ref. [CHH15] as  $k_2 = s_w^2 * c_2$  and  $k_1 = c_w^2 * c_1$ .

**[TODO: Linda will possibly complete/correct this paragraph]**  
UV completions of such operators where the dominant signature

is a single photon or EW boson are possible, for example through the exchange of a  $W'$  or a  $Z'$ . They are left as benchmarks for future searches as their implementation may require loop diagrams and need further studies beyond the timescale of this Forum.

As shown in Fig. 4.4 kinematics of this model can be approximated by that of a simplified model including a high-mass scalar mediator exchanged in the s-channel. For this reason, the list of benchmark models with direct boson-DM couplings only includes dimension 7 operators. **[TODO: then we need to recommend the scalar mediator, but then the sensitivity is very poor wrt monojets - however, I still prefer to generate a few (high-mass) simplified model points wrt an EFT if given the choice.]**



Figure 4.4: Comparison of the missing transverse momentum for the simplified model where a scalar mediator is exchanged in the s-channel and the model including a dimension-5 scalar contact operator, in the leptonic Z+MET final state

The kinematic distributions for dimension-7 scalar and pseudoscalar operators only shows small differences, as shown in Fig. 4.5.



Figure 4.5: Comparison of the missing transverse momentum for the scalar and pseudoscalar operators with direct interaction between DM and photon, in the photon+MET final state

Similarly, the differences in kinematics for the various signatures are negligible when changing the coefficients  $k_1$  and  $k_2$ , as shown in Figure ?? . Only the case  $k_1 = k_2 = 1$  is generated as benchmark; other cases are left for reinterpretation as they will only need a rescaling of the cross-sections shown in Table ?? **[TODO: add tables with cross sections]** for the various Dark Matter mass points considered.

Examples of relevant kinematic distributions for selected benchmark points are shown in Fig. 4.7.



(a) Missing transverse momentum distribution for the photon+MET final state.



(b) Missing transverse momentum distribution for the leptonic Z+MET final state.



(c) Transverse mass ( $m_T$ ) for the leptonic W+MET final state.

Figure 4.6: Kinematic distributions relevant for searches with W, Z and photons in the final state, for for the scalar and pseudoscalar operators representing direct interactions between DM and bosons.

### 545 4.3 *Specific simplified models*

546 Mono-Higgs, to be completed...





(a) Missing transverse momentum distribution for the photon+MET final state.



(b) Missing transverse momentum distribution for the leptonic Z+MET final state.



(c) Transverse mass ( $m_T$ ) for the leptonic W+MET final state.



(d) Fat **[Insert algorithm]** jet mass ( $m_T$ ) for the the hadronic W+MET final state.

Figure 4.7: Kinematic distributions relevant for searches with W, Z and photons in the final state, for the simplified model with a vector mediator exchanged in the  $s$ -channel.



## Specific models for signatures with heavy flavor quarks

5.0.1 Specific models for analyses of MET+b quark(s)

5.0.2  $b\bar{b}$ +MET models

5.0.3 Models with a single b-quark + MET

5.1 Specific models for analyses of MET+top quark(s)

5.1.1  $t\bar{t}$ +MET models

5.2 Models with a single top-quark + MET

**[TODO: find a consistent notation for  $X_{\text{new}}$ ,  $M$ ,  $V$  and Madgraph model]**

A dark matter candidate  $\chi$  and a new particle  $M$  (vector or scalar) are added to the SM, in an effective theory that respects the  $SU(2)_L \times U(1)_Y$  symmetry and produces a single top quark in association with either the DM particle or the new particle (generally called  $X_{\text{new}}$  when no distinction is made). The full details of these models are described in [AFM11, AAB<sup>+</sup>14, BCDF15].

There are two classes of models based on the monotop production mode: resonant and non-resonant production, as shown in Fig. 5.1.

The following two sections describe the phenomenology leading to these two production mechanisms. Depending on the nature of  $X_{\text{new}}$ , two main final states might be relevant: monotop production or same-sign top quark pair production. The interplay of these two signatures can largely probe this class of dark matter model, but a detailed study of their complementarity is beyond the scope of this Forum report.

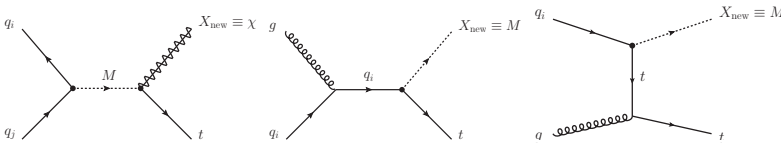


Figure 5.1: Feynman diagram of leading order processes leading to monotop events: resonant production of  $t$  via resonant new particle  $M$  decaying into a top quark and  $X_{\text{new}}$ , which is the dark matter fermion  $\chi$  (left), and  $s$  and  $t$  channel non-resonant production of a top quark in association with  $X_{\text{new}}$ , which is the new particle  $M$  (middle and right).

## 572 RESONANT PRODUCTION

573 In this case, the new particle  $M$  is a coloured 2/3-charged scalar  
 574  $\phi^\pm$  decaying into a top quark and a spin-1/2 invisible particle,  $\chi$  (in  
 575 this case  $X_{\text{new}}$  is the dark matter candidate  $\chi$ ). The dynamics of the  
 576 new sector is then described by the following Lagrangian:

$$\mathcal{L} = d_i^C [(g_{\phi d}^v)^{ij} + (g_{\phi d}^a)^{ij} \gamma^5] d_j \phi^\pm + u_k^C [(g_{u\chi}^v)^k + (g_{u\chi}^a)^k \gamma^5] \chi \phi^\pm \quad (5.1)$$

577 where  $u$  ( $d$ ) stands for any  $up$ -quark ( $down$ -quark), the index  $v$  ( $a$ )  
 578 stands for vectorial (axial),  $C$  means charge conjugate and  $i, j, k$  run  
 579 over the generations (color indices involved in the  $\phi^\pm$ -quarks in-  
 580 teraction are not explicitly written). The first term leads to the pro-  
 581 duction of the new particle and the last term allows its decay into  
 582 a  $up$ -quark and a non interacting fermion (in particular to the top  
 583 quark when  $(g_{u\chi}^{v/a})^k$  is sizable mainly for  $k = 3$ ). This model is then  
 584 described by the masses of the new particle  $m_\phi$  and the invisible  
 585 fermion  $m_\chi$ , and the coupling  $(g_{\phi d}^{v/a})^{ij}$  and  $(g_{u\chi}^{v/a})^k$ .

## 586 NON-RESONANT PRODUCTION

587 For the non-resonant production, the top quark is produced in  
 588 association with the new particle ( $X_{\text{new}}$  is then the new particle and  
 589 not the dark matter candidate). The new particle can be either a new  
 590 scalar, interacting with the SM and the DM candidate, or a new vec-  
 591 tor. For simplicity, we only consider the case of a vector new particle,  
 592 as the scalar case would involve a mixing with the SM Higgs boson  
 593 and therefore a larger parameter space.

The dynamics of a case with a vector new particle follows this  
 Lagrangian:

$$\mathcal{L} = \bar{u}_i [(g_{Vu}^v)^{ij} \gamma^\mu + (g_{Vu}^a)^{ij} \gamma^5] u_j V_\mu + \bar{\chi} [g_{V\chi}^v \gamma^\mu + g_{V\chi}^a \gamma^5] \chi V_\mu \quad (5.2)$$

594 where  $u$  stands for any  $up$ -quark, the index  $v$  ( $a$ ) stands for vectorial  
 595 (axial) and  $i, j, k$  run over the generations. The first term describes  
 596 the interaction between the new particle and the  $up$ -quarks while  
 597 the second term leads to the decay the new particle into invisible  
 598 fermions. The new sector can be defined with the couplings  $(g_{Vu}^{v/a})^{ij}$ ,  
 599  $g_{V\chi}^{a/v}$  and the masses  $m_V$  and  $m_\chi$ . This model can be probed by two  
 600 different experimental signatures: monotop and same-sign top quark  
 601 production.

## 602 MODEL PARAMETERS AND ASSUMPTIONS

603 The models considered as benchmarks for the first LHC searches  
 604 contain further assumptions in terms of the flavour and chiral struc-  
 605 ture of the model with respect to the full Lagrangians from equa-  
 606 tions (5.1) and (5.2). These assumptions lead to limitations in LHC

constraints of the parameter space of these models, qualitatively discussed below.

*Assumptions in the flavour structure of the models* In order to be visible at the LHC in the monotop final state, these models must include a strong coupling between the new particle  $\phi$  and  $t\chi$ . In the resonant case, the new particle must also couple to light quarks in order to be produced at the LHC, leading to possible constraints from dijet searches. The same kind of assumption exists for the non-resonant production. The new particle  $M$  must be produced from a light quark in the initial state, in association with a top quark: this signature can mainly probe a high coupling  $\left(g_{Vu}^{v/a}\right)_{Vu}^{13} \equiv g_{Vtu}^{v/a}$ . Therefore, the sensitivity to other flavour couplings is significantly lower, since  $V$  would be produced at a lower rate.

*Assumptions in the chiral structure of the models* We only consider right-handed quark components, in order to simplify the phenomenology. The representation of the left-handed components under the  $SU(2)_L$  symmetry would add a coupling to *down*-type quarks, since the effective theory is invariant under  $SU(2)_L \times U(1)_Y$  gauge symmetry. Having a coupling between the new particle and *down*-type quarks complicates the collider phenomenology in terms of decay modes. Typically, including the left-handed components of quarks in the lagrangian (5.2) describing the  $Vtu$  vertex would lead to

$$\mathcal{L}_{Vtu} = g_{Vtu}^R \bar{t}_R \gamma^\mu u_R V_\mu + g_{Vtu}^L (\bar{t}_L \gamma^\mu u_L + \bar{b}_L \gamma^\mu d_L) V_\mu \quad (5.3)$$

where  $g^{R/L} \equiv 1/2 (g^v \pm g^a)$  couples only to right-handed/left-handed components. The second term stems from invariance under  $SU(2)_L$  rotations, and leads to an additional decay mode  $V \rightarrow b\bar{d} + \bar{b}d$  (on top of  $V \rightarrow t\bar{u} + \bar{t}u$  and  $V \rightarrow \chi\chi$ ). **[Open point: do we just set the 2nd term to zero in this model? Justification?]**

## IMPLEMENTATION AND NOTATION

This Section describes the notations used in the MadGraph model [Fuk] convention, in term of the ones introduced in the previous Section.

The Madgraph model corresponds to the Lagrangian from [AFM11]. Each coupling constant of this dynamics can be set via the parameter card and the blocks which are relevant for the two models used for the experimental searches are described below.

### 1. Resonant scalar model described by the Lagrangian (5.1)

- AQS and BQS:  $3 \times 3$  matrices (flavour space) fixing the coupling of the scalar  $\phi^\pm$  ( $S$  stands for scalar) and *down*-type quarks ( $Q$  stands for quarks), written in this note  $g_{\phi u}$  or  $a_{\text{res}}^q$ .

- A12S and B12S:  $3 \times 1$  matrices (flavour space) fixing the coupling of the fermion  $\chi$  (12 stands for spin-1/2 fermion) and  $up$ -type quarks, written in this note  $g_{u\chi}$  or  $a_{\text{res}}^{1/2}$ .

- particle name: the scalar  $\phi^\pm$  is labelled  $S$  and the fermion  $\chi$  is  $f_{\text{met}}$

## 2. Non-resonant vectorial model described by the Lagrangian (5.2)

- A1FC and B1FC:  $3 \times 3$  matrices (flavour space) fixing the coupling of the vector  $V$  (1 stands for vector) and  $up$ -type quarks, written in this note  $g_{Vu}$  or  $a_{\text{non-res}}$ .

- particle name: the vector  $V$  is labelled  $v_{\text{met}}$  and the fermion  $\chi$  doesn't exist

- the dark matter candidate  $\chi$  is not implemented (this model assumes  $\text{BR}(V \rightarrow \chi\chi) = 100\%$ )

$A$  means vectorial coupling ( $g^v$ ) and  $B$  means axial coupling ( $g^a$ ) and these two matrices are taken to be equal according to the chiral assumptions made above. The convention adopted follows [ATL15] in defining a single number  $a_{\text{res}}$  ( $a_{\text{non-res}}$ ) for the resonant (non resonant) model, such as  $(a_{\text{res}}^q)_{12} = (a_{\text{res}}^q)_{21} = (a_{\text{res}}^{1/2})_3 \equiv a_{\text{res}}$  (in order to have  $d - s - S$  couplings, and  $t - S - f_{\text{met}}$  couplings) and  $(a_{\text{non-res}})_{13} = (a_{\text{non-res}})_{31} \equiv a_{\text{non-res}}$  (in order to have  $v_{\text{met}} - t - u$  couplings).

## PARAMETER SCAN

### [Open point - parameter scan studies go here.]

Which parameters impact the kinematics (this is the only relevant aspect from the experimental point of view)? Some studies would be nice to put in this documents about:

- mediator mass
- mediator width: no effect (or parametrizable effects, plots are ready and need to be included)
- **which parameters** impact our experimental sensitivity? Which plane should be scanned?

What are the relevant numerical range to explore? First guess would be to follow the mono-top analysis.

## PARAMETER CHOICES AND CROSS SECTIONS

### [Open point: update with new numbers]

ATLAS has considered two models, a resonant and a non-resonant production, using only right-handed top quarks in the lepton+jets

final state. The signal samples were produced with MADGRAPH5 v1.5.11 interfaced with PYTHIA 8.175, using the MSTW2008LO Parton Distribution Function (PDF) set (lhpdf ID: 21000). The mass of the top quark was set at 172.5 GeV. Dynamic renormalisation and factorisation scales were used. The  $MET$  particle mass was varied, and in the case of the resonant model the resonance mass was fixed at 500 GeV:

- Resonant model,  $MET$  particle mass: [0,100] GeV in 20 GeV steps
- Non-resonant model,  $MET$  particle mass: [0,150] GeV in 25 GeV steps, [200,300] GeV in 50 GeV and [400,1000] GeV in 100 GeV steps

The couplings  $a_{\text{res}}$  and  $a_{\text{non-res}}$  are set at a fixed value of 0.2. In addition, two samples are produced for the resonant model for  $m(f_{\text{met}}) = 100$  GeV, with coupling strengths fixed at  $a_{\text{res}} = 0.5$  and  $a_{\text{res}} = 1.0$ , in order to check the effect of the resonance width on the signal event kinematics. The total width of the resonance varies quadratically with the coupling strength, corresponding to a width of 3.5 GeV, 21.6 GeV, and 86.5 GeV at  $a_{\text{res}} = 0.2$ ,  $a_{\text{res}} = 0.5$ , and  $a_{\text{res}} = 1.0$ , respectively.

The number of free parameters is reduced by assuming  $(a_{\text{res}}^q)_{12} = (a_{\text{res}}^q)_{21} = (a_{\text{res}}^{1/2})_3 \equiv a_{\text{res}}$  for the resonant model and  $(a_{\text{non-res}})_{13} = (a_{\text{non-res}})_{31} \equiv a_{\text{non-res}}$  for the non-resonant model, all other elements of these coupling matrices being equal to 0. For each model, the coupling parameter  $a_{\text{res}}$  or  $a_{\text{non-res}}$  and the masses of the exotic particles are independent.

The cross-sections as well as the width of the resonance for the resonance model are shown in Table 5.1. The cross-section is slowly decreasing when  $m(f_{\text{met}})$  increases, and the values do not differ by larger than 10%, due to the similarity of the kinematics, in the chosen mass range.

$m(f_{\text{met}})$ [GeV]	$\sigma_{\text{lep}}$ [pb]	$\sigma_{\text{had}}$ [pb]	$\Gamma(\Phi)$ [GeV]
0	1.107	2.214	3.492
20	1.102	2.205	3.491
40	1.089	2.180	3.487
60	1.068	2.137	3.481
80	1.039	2.078	3.472
100	1.001	2.003	3.461
100 ( $a_{\text{res}} = 0.5$ )	6.091	12.13	21.63
100 ( $a_{\text{res}} = 1.0$ )	21.77	43.72	86.52

Table 5.1: Theoretical predictions for the product of the production cross-section of the scalar resonance, the branching ratio of its decay into a top quark and the invisible particle, and of the branching ratio of the top quark decay into a semi-leptonic ( $\sigma_{\text{lep}}$ ) or fully-hadronic ( $\sigma_{\text{had}}$ ) final state, in the resonance model. Values are given for a resonance of mass 500 GeV and for an effective coupling  $a_{\text{res}} = 0.2$  (except for two masses), as a function of the mass  $m(f_{\text{met}})$  of the neutral fermion. The total widths  $\Gamma(\Phi)$  of the resonance are also shown.

For the non-resonant case, the cross-sections are given in Table 5.2 and are calculated with  $a_{\text{non-res}} = 0.2$ . The cross-section diverges

when  $m(v_{met})$  tends to 0 GeV. However, when the mass is exactly 0 GeV the cross-section has a finite value, due to the specificity of the propagator for this massless spin-1 boson.

$m(v_{met})$ [GeV]	$\sigma_{lep}$ [pb]	$\sigma_{had}$ [pb]
0	96.03	192.4
25	359.0	717.9
50	113.4	226.9
75	59.86	119.5
100	37.45	74.82
125	25.35	50.68
150	18.00	35.96
200	9.662	19.28
250	5.506	11.02
300	3.328	6.656
400	1.372	2.738
500	0.6345	1.270
600	0.3192	0.6354
700	0.1698	0.3383
800	0.09417	0.1883
900	0.05472	0.1091
1000	0.03259	0.06479

Table 5.2: Theoretical predictions for the product of the production cross-section of the invisible vector  $v_{met}$  and of a top quark, and of the branching ratio of the top quark decay into a semi-leptonic ( $\sigma_{lep}$ ) or fully-hadronic ( $\sigma_{had}$ ) final state, in the non-resonance model. Values are given for an effective coupling  $a_{non-res} = 0.2$ , as a function of the mass  $m(v_{met})$  of the invisible state.

[Open point: systematic uncertainties]



## Validity of EFT approach

Effective Field Theories (EFTs) are an extremely useful tool for DM searches at the LHC. Given the current lack of indications about the nature of the DM particle and its interactions, a model independent interpretation of the collider bounds appears mandatory, especially in complementarity with the reinterpretation of the exclusion limits within a choice of simplified models, which cannot exhaust the set of possible completions of an effective Lagrangian. However EFTs must be used with caution at LHC energies, where the energy scale of the interaction is at a scale where the EFT approximation can no longer be assumed to be valid. Here we summarise some methods that can be used to ensure the validity of the EFT approximation. These methods are described in detail in Refs. [BDSMR14<sup>?</sup>, BDSJ<sup>+</sup>14, A<sup>+</sup>15, RWZ15].

### Outline of the procedure described in Refs. [A<sup>+</sup>15]

For a tree-level interaction between DM and the Standard Model (SM) via some mediator with mass  $M$ , the EFT approximation corresponds to expanding the propagator in powers of  $Q_{\text{tr}}^2/M^2$ , truncating at lowest order, and combining the remaining parameters into a single parameter  $M_*$  (also called  $\Lambda$ ). For an example scenario with a  $Z'$ -type mediator (leading to some combination of operators D5 to D8 in the EFT limit) this corresponds to setting

$$\frac{g_{\text{DM}}g_q}{Q_{\text{tr}}^2 - M^2} = -\frac{g_{\text{DM}}g_q}{M^2} \left( 1 + \frac{Q_{\text{tr}}^2}{M^2} + \mathcal{O}\left(\frac{Q_{\text{tr}}^4}{M^4}\right) \right) \simeq -\frac{1}{M_*^2}, \quad (6.1)$$

where  $Q_{\text{tr}}$  is the momentum carried by the mediator, and  $g_{\text{DM}}, g_q$  are the DM-mediator and quark-mediator couplings respectively. Similar expressions exist for other operators. Clearly the condition that must be satisfied for this approximation to be valid is that  $Q_{\text{tr}}^2 < M^2 = g_{\text{DM}}g_q M_*^2$ .

We can use this condition to enforce the validity of the EFT approximation by restricting the signal (after the imposition of the cuts

of the analysis) to events for which  $Q_{\text{tr}}^2 < M^2$ . This truncated signal can then be used to derive the new, truncated limit on  $M_*$  as a function of  $(m_{\text{DM}}, g_{\text{DM}} g_q)$ .

For the example D5-like operator,  $\sigma \propto M_*^{-4}$ , and so there is a simple rule for converting a rescaled cross section into a rescaled constraint on  $M_*$  if the original limit is based on a simple cut-and-count procedure. Defining  $\sigma_{\text{EFT}}^{\text{cut}}$  as the cross section truncated such that all events pass the condition  $\sqrt{g_{\text{DM}} g_q} M_*^{\text{rescaled}} > Q_{\text{tr}}$ , we have

$$M_*^{\text{rescaled}} = \left( \frac{\sigma_{\text{EFT}}}{\sigma_{\text{EFT}}^{\text{cut}}} \right)^{1/4} M_*^{\text{original}}, \quad (6.2)$$

which can be solved for  $M_*^{\text{rescaled}}$  via either iteration or a scan (note that  $M_*^{\text{rescaled}}$  appears on both the LHS and RHS of the equation). Similar relations exist for a given UV completion of each operator. The details and application of this procedure to ATLAS results can be found in Ref. [A<sup>+</sup>15] for a range of operators. Since this method uses the physical couplings and energy scale  $Q_{\text{tr}}$ , it gives the strongest possible constraints in the EFT limit while remaining robust by ensuring the validity of the EFT approximation.

*Outline of the procedure described in Ref. [RWZ15]*

In [RWZ15] a procedure to extract model independent and consistent bounds within the EFT is described. This procedure can be applied to any effective Lagrangian describing the interactions between the DM and the SM, and provides limits that can be directly reinterpreted in any completion of the EFT.

The range of applicability of the EFT is defined by a mass scale  $M_{\text{cut}}$ , a parameter which marks the upper limit of the range of energy scales at which the EFT can be used reliably, independently of the particular completion of the model. Regardless of the details of the full theory, the energy scale probing the validity of the EFT is less than or equal to the centre-of-mass energy  $E_{\text{cm}}$ , the total invariant mass of the hard final states of the reaction. Therefore, the condition ensuring the validity of the EFT is, by definition of  $M_{\text{cut}}$ ,

$$E_{\text{cm}} < M_{\text{cut}}. \quad (6.3)$$

For example, in the specific case of a tree level mediation with a single mediator,  $M_{\text{cut}}$  can be interpreted as the mass of that mediator.

There are then at least three free parameters describing an EFT: the DM mass  $m_{\text{DM}}$ , the scale  $M_*$  of the interaction, and the cutoff scale  $M_{\text{cut}}$ .

We can use the same technique as above to restrict the signal to the events for which  $E_{\text{cm}} < M_{\text{cut}}$ , using only these events to derive the exclusion limits on  $M_*$  as a function of  $(m_{\text{DM}}, M_{\text{cut}})$ . We can also define an *effective coupling strength*  $M_{\text{cut}} = g_* M_*$ , where  $g_*$  is a free parameter that substitutes the parameter  $M_{\text{cut}}$ , and therefore derive exclusions on  $M_*$  as a function of  $(m_{\text{DM}}, g_*)$ . This allows us to see how much of the theoretically allowed parameter space has been actually tested and how much is still unexplored; For example, in the  $Z'$ -type model considered above,  $g_*$  is equal to  $\sqrt{g_{\text{DM}} g_q}$ . The resulting plots are shown in [RWZ15] for a particular effective operator.

The advantage of this procedure is that the obtained bounds can be directly and easily recast in any completion of the EFT, by computing the parameters  $M_*$ ,  $M_{\text{cut}}$  in the full model as functions of the parameters of the complete theory. On the other hand, the resulting limits will be weaker than those obtained using  $Q_{\text{tr}}$  and a specific UV completion.



770 *A*

771 *Appendix: Detailed studies on mono-jet signatures*



## B

### Appendix: Detailed studies for EW models

#### B.1 Further W+MET models with possible cross-section enhancements

As pointed out in Ref. [BCD<sup>+</sup>15], the mono- $W$  signature can probe the iso-spin violating interactions of dark matter with quarks. The relevant operators after the electroweak symmetry breaking is

$$\frac{1}{\Lambda^2} \bar{\chi} \gamma_\mu \chi (\bar{u}_L \gamma^\mu u_L + \xi \bar{d}_L \gamma^\mu d_L) . \quad (\text{B.1})$$

Here, we only keep the left-handed quarks because the right-handed quarks do not radiate a  $W$ -gauge boson from the weak interaction. As the LHC constraints the cutoff to higher values, it is also important to know the corresponding operators before the electroweak symmetry. At the dimension-six level, the following operator

$$\frac{c_6}{\Lambda^2} \bar{\chi} \gamma_\mu \chi \bar{Q}_L \gamma^\mu Q_L \quad (\text{B.2})$$

conserves iso-spin and provides us  $\xi = 1$  [? ]. At the dimension-eight level, new operators appear to induce iso-spin violation and can be

$$\frac{c_8^d}{\Lambda^4} \bar{\chi} \gamma_\mu \chi (H \bar{Q}_L) \gamma^\mu (Q_L H^\dagger) + \frac{c_8^u}{\Lambda^4} \bar{\chi} \gamma_\mu \chi (\tilde{H} \bar{Q}_L) \gamma^\mu (Q_L \tilde{H}^\dagger) . \quad (\text{B.3})$$

After inputting the vacuum expectation value of the Higgs field, we have

$$\xi = \frac{c_6 + c_8^d v_{\text{EW}}^2 / 2\Lambda^2}{c_6 + c_8^u v_{\text{EW}}^2 / 2\Lambda^2} . \quad (\text{B.4})$$

For a nonzero  $c_6$  and  $v_{\text{EW}} \ll \Lambda$ , the iso-spin violation effects are suppressed. On the other hand, the values of  $c_6$ ,  $c_8^d$  and  $c_8^u$  depend on the UV-models.

There is one possible UV-model to obtain a zero value for  $c_6$  and non-zero values for  $c_8^d$  and  $c_8^u$ . One can have the dark matter and the SM Higgs field charged under a new  $U(1)'$ . There is a small mass mixing between SM  $Z$ -boson and the new  $Z'$  with a mixing angle

of  $\mathcal{O}(v_{\text{EW}}^2/M_{Z'}^2)$ . After integrating out  $Z'$ , one has different effective dark matter couplings to  $u_L$  and  $d_L$  fields, which are proportional to their couplings to the  $Z$  boson. For this model, we have  $c_6 = 0$  and

$$\tilde{\zeta} = \frac{-\frac{1}{2} + \frac{1}{3} \sin^2 \theta_W}{\frac{1}{2} - \frac{2}{3} \sin^2 \theta_W} \approx -2.7 \quad (\text{B.5})$$

779 and order of unity.



## Bibliography

- [A<sup>+</sup>14a] Georges Aad et al. Search for new particles in events with one lepton and missing transverse momentum in  $pp$  collisions at  $\sqrt{s} = 8$  TeV with the ATLAS detector. *JHEP*, 1409:037, 2014.
- [A<sup>+</sup>14b] Jalal Abdallah et al. Simplified Models for Dark Matter and Missing Energy Searches at the LHC. *arXiv:1409.2893*, 2014.
- [A<sup>+</sup>15] Georges Aad et al. Search for new phenomena in final states with an energetic jet and large missing transverse momentum in  $pp$  collisions at  $\sqrt{s} = 8$  TeV with the ATLAS detector. 2015.
- [AAB<sup>+</sup>14] Jean-Laurent Agram, Jeremy Andrea, Michael Buttignol, Eric Conte, and Benjamin Fuks. Monotop phenomenology at the Large Hadron Collider. *Phys.Rev.*, D89(1):014028, 2014.
- [Aad14a] Search for dark matter in events with a hadronically decaying W or Z boson and missing transverse momentum in  $pp$  collisions at  $\sqrt{s} = 8$  TeV with the ATLAS detector. *Phys.Rev.Lett.*, 112(4):041802, 2014.
- [Aad14b] Search for dark matter in events with a Z boson and missing transverse momentum in  $pp$  collisions at  $\sqrt{s}=8$  TeV with the ATLAS detector. *Phys.Rev.*, D90(1):012004, 2014.
- [Aad15] Search for new phenomena in events with a photon and missing transverse momentum in  $pp$  collisions at  $\sqrt{s} = 8$  TeV with the ATLAS detector. *Phys.Rev.*, D91(1):012008, 2015.
- [AFM11] J. Andrea, B. Fuks, and F. Maltoni. Monotops at the LHC. *Phys.Rev.*, D84:074025, 2011.

- [ATL14] Sensitivity to WIMP Dark Matter in the Final States Containing Jets and Missing Transverse Momentum with the ATLAS Detector at 14 TeV LHC. Technical Report ATL-PHYS-PUB-2014-007, CERN, Geneva, Jun 2014.
- [ATL15] Search for a single-top quark produced in association with missing energy in proton-proton collisions at  $\sqrt{s} = 8$  TeV with the ATLAS detector. *Eur. Phys. J. C*, 75:79, 2015.
- [AWZ14] Haipeng An, Lian-Tao Wang, and Hao Zhang. Dark matter with  $t$ -channel mediator: a simple step beyond contact interaction. *Phys. Rev. D*, 89:115014, 2014.
- [BB13] Yang Bai and Joshua Berger. Fermion Portal Dark Matter. *JHEP*, 11:171, 2013.
- [BCD<sup>+</sup>15] Nicole F. Bell, Yi Cai, James B. Dent, Rebecca K. Leane, and Thomas J. Weiler. Dark matter at the LHC: EFTs and gauge invariance. 2015.
- [BCDF15] Idir Boucheneb, Giacomo Cacciapaglia, Aldo Deandrea, and Benjamin Fuks. Revisiting monotop production at the LHC. *JHEP*, 1501:017, 2015.
- [BDSJ<sup>+</sup>14] Giorgio Busoni, Andrea De Simone, Thomas Jacques, Enrico Morgante, and Antonio Riotto. On the Validity of the Effective Field Theory for Dark Matter Searches at the LHC Part III: Analysis for the  $t$ -channel. *JCAP*, 1409:022, 2014.
- [BDSMR14] Giorgio Busoni, Andrea De Simone, Enrico Morgante, and Antonio Riotto. On the Validity of the Effective Field Theory for Dark Matter Searches at the LHC. *Phys.Lett.*, B728:412–421, 2014.
- [BT13] Yang Bai and Tim M.P. Tait. Searches with Mono-Leptons. *Phys.Lett.*, B723:384–387, 2013.
- [CDM<sup>+</sup>14] Linda Carpenter, Anthony DiFranzo, Michael Mulhearn, Chase Shimmin, Sean Tulin, et al. Mono-Higgs-boson: A new collider probe of dark matter. *Phys.Rev.*, D89(7):075017, 2014.
- [CEHL14] Spencer Chang, Ralph Edezhath, Jeffrey Hutchinson, and Markus Luty. Effective WIMPs. *Phys. Rev. D*, 89:015011, 2014.

- [CHH15] Andreas Crivellin, Ulrich Haisch, and Anthony Hibbs. LHC constraints on gauge boson couplings to dark matter. 2015.
- [CHLR13] R.C. Cotta, J.L. Hewett, M.P. Le, and T.G. Rizzo. Bounds on Dark Matter Interactions with Electroweak Gauge Bosons. *Phys.Rev.*, D88:116009, 2013.
- [CNS<sup>+</sup>13] Linda M. Carpenter, Andrew Nelson, Chase Shimmin, Tim M.P. Tait, and Daniel Whiteson. Collider searches for dark matter in events with a Z boson and missing energy. *Phys.Rev.*, D87(7):074005, 2013.
- [DNRT13] Anthony DiFranzo, Keiko I. Nagao, Arvind Rajaraman, and Tim M. P. Tait. Simplified Models for Dark Matter Interacting With Quarks. *JHEP*, 1311, 2013.
- [Fuk] Benjamin Fuks. Monotop Effective Theory: MadGraph model. <http://feynrules.irmp.ucl.ac.be/wiki/Monotops>.
- [GIR<sup>+</sup>10] Jessica Goodman, Masahiro Ibe, Arvind Rajaraman, William Shepherd, Tim M.P. Tait, et al. Constraints on Dark Matter from Colliders. *Phys.Rev.*, D82:116010, 2010.
- [HK11] Robert M. Harris and Konstantinos Kousouris. Searches for dijet resonances at hadron colliders. *Int. J. Modern Phys.*, 26(30n31):5005–5055, 2011.
- [HKR13] Ulrich Haisch, Felix Kahlhoefer, and Emanuele Re. QCD effects in mono-jet searches for dark matter. *JHEP*, 1312:007, 2013.
- [HR15] Ulrich Haisch and Emanuele Re. Simplified dark matter top-quark interactions at the LHC. 2015.
- [K<sup>+</sup>14] Vardan Khachatryan et al. Search for physics beyond the standard model in final states with a lepton and missing transverse energy in proton-proton collisions at  $\sqrt{s} = 8$  TeV. 2014.
- [Kha14] Search for new phenomena in monophoton final states in proton-proton collisions at  $\sqrt{s} = 8$  TeV. 2014.
- [NCC<sup>+</sup>14] Andy Nelson, Linda M. Carpenter, Randel Cotta, Adam Johnstone, and Daniel Whiteson. Confronting the Fermi Line with LHC data: an Effective Theory of Dark Matter Interaction with Photons. *Phys.Rev.*, D89(5):056011, 2014.

- [PVZ<sub>14</sub>] Michele Papucci, Alessandro Vichi, and Kathryn M. Zurek. Monojet versus the rest of the world I:  $t$ -channel models. *JHEP*, 2014.
- [RWZ<sub>15</sub>] Davide Racco, Andrea Wulzer, and Fabio Zwirner. Robust collider limits on heavy-mediator Dark Matter. 2015.
- [ZBW<sub>13</sub>] Ning Zhou, David Berge, and Daniel Whiteson. Mono-everything: combined limits on dark matter production at colliders from multiple final states. *Phys.Rev.*, D87(9):095013, 2013.

